Peer Reviewed Paper openaccess Paper Presented at IASIM 2022, July 2022, Esbjerg, Denmark

Estimation of pigment concentration in LDPE via in-line hyperspectral imaging and machine learning

Georgiana Amariei,[a] Anne Sofie Schaarup-Kjær,[a,b] Pernille Klarskov,[c] Martin Lahn Henriksen[a] and Mogens Hinge[a,*]

[a]Plastic and Polymer Engineering, Department of Biological and Chemical Engineering, Aarhus University, Aabogade 40, DK-8200 Aarhus N., Denmark

[b]American AVK Company, Quality Department, 2155 Meridian Blvd, Minden, NV 89423, USA

[c]Terahertz Photonics, Department of Electrical and Computer Engineering, Aarhus University, Finlandsgade 22, DK-8200, Aarhus N, Denmark

Contact
G. Amariei: georgiana.amariei@bce.au.dk
https://orcid.org/0000-0002-5412-6325
A.S. Schaarup-Kjær: sofie.schaarupk@gmail.com
https://orcid.org/0000-0003-3458-166X
P. Klarskov: klarskov@ece.au.dk
https://orcid.org/0000-0002-9422-7841
M.L. Henriksen: lahn@bce.au.dk
https://orcid.org/0000-0002-5115-6166
M. Hinge: hinge@bce.au.dk
https://orcid.org/0000-0002-8787-5314

Due to the increasing amount of plastic waste and high-quality demands on recycled plastic interest for in-line composition estimation in plastics has grown the last few years. This study investigates pigment blue 15 : 3 with varying concentrations in LDPE. Samples are investigated with two industrial hyperspectral imaging systems where one has the hyperspectral range from 450 nm to 1050 nm and the other from 950 nm to 1750 nm. A model based on peak ratios of selected bands and model based on a principal component analysis have been tested. The models only predict pigment concentrations between 40.0 wt% and 1.7 × 10^{-3} wt% if both spectral ranges are combined. Unknown samples containing pigment concentration ranging from 20 wt% to 0.31 wt% were predicted and correlated to the actual pigment concentrations ($R^2 = 0.977$) and the PC-based model outperforms the peak ratio model. The studied approach can be a part of the solution to the plastic challenge and can be transferred to other applications where concentration determination is key.

Keywords: hyperspectral imaging, pigment blue 15:3, pigment concentration, in-line concentration estimation, machine learning

Introduction

Plastics material are applied all over modern society and only a minor amount of the consumer plastics is included into the plastic circular economy and thus into new products.[1–4] This fact and the insufficient (or lacking) waste management has resulted in plastic accumulation in our ecosystems.[5–11] There are currently many unsolved challenges in plastic recycling, e.g. poor waste management, consumer behaviour, multi material designs etc.[12,13] Hence plastics arriving for recycling is a complex mixture of sizes, materials and colours. This challenges the

Correspondence
M. Hinge: hinge@bce.au.dk

Received: 20 October 2022
Revised: 27 November 2022
Accepted: 27 November 2022
Publication: 3 April 2023
doi: 10.1255/jsi.2023.a2
ISSN: 2040-4565

Citation
G. Amariei, A.S. Schaarup-Kjær, P. Klarskov, M.L. Henriksen and M. Hinge, "Estimation of pigment concentration in LDPE via in-line hyperspectral imaging and machine learning", *J. Spectral Imaging* **12,** a2 (2023). https://doi.org/10.1255/jsi.2023.a2

necessary 95 %+ material purity for recycled plastics in high value products.[14] In addition, the complex colour mix in post-consumer plastics results in most recycled plastic pellets being dyed black at the recyclers. This limits the potential usage of recycled plastic and it would be beneficial if the pigment composition and concentrations of the incoming plastic materials could be obtained and utilised during plastic sorting.

Pigments can be detected via different chemical-based techniques, such as high-performance liquid chromatography, gas chromatography, liquid chromatography-mass spectrometry, analytical pyrolysis coupled with gas chromatography-mass spectrometry and/or inductively coupled plasma mass spectrometry.[15,16] These methods are accurate but require time-consuming sample preparation, a long analysis time (minutes/hours), relatively small sampling volumes and highly-skilled operators.

As an alternative optical analytical methods is a potential solution for pigments detection, such as Fourier-transform infrared (FT-IR) spectroscopy,[17–19] visible and near infrared spectroscopy (Vis/NIR),[20,21] Raman spectroscopy[22–24] and fluorescence spectroscopy.[25] However, these spectroscopic techniques only analyse a minor part of the sample and analysis handling and time for detection is relatively long (seconds to minutes).

For faster and larger sampling area, line-scan-based hyperspectral imaging (HSI) technologies that provide spatial information can be applied. HSI is emerged as a powerful analysis tool for rapid and non-destructive detection applied in agricultural,[26–28] medicinal industry,[29] waste streams[30] and plastics.[30–34] In addition, HSI has been successfully applied in determining pigments, binders, canvas material etc. in relation to art heritage preservation[35–39] by applying cameras covering wavelengths from 400 nm to 2500 nm, hence covering both visible (Vis) and short-wave infrared ranges (SWIR). However, the experimental setup is highly specialised and designed for scanning of art pieces.

Due to the vast amount of data obtained via HSI the above studies apply some type of machine learning [principal component analysis (PCA), K-Nearest Neighbour regression, K-means clustering, partial least square regression (PLSR), multiple linear regression (MLR), support vector regression (SVR), spectral correlation measurement etc.] or neural network (NN) for data processing. Random forest and NN model estimated the phycocyanin and Chlorophyll-*a* (Chl-*a*) pigments in cyanobacteria within the concentration ranges of 1.47×10^{-5}–1.90×10^{-8} wt% and 1.11×10^{-5}–8.45×10^{-7} wt%, respectively.[40] SVR, MLR and PLSR algorithms using both a full spectra and selected effective-wavelengths were applied to predict 0.62–0.35 wt% lipid concentrations in algae,[41] 0.33–0.17 wt% Chl-*a* and 0.06–0.03 wt% carotenoid in cucumber leaves,[42] 0.33–0.01 wt% anthocyanin content of grapes[43–45] and 0.03–0.01 wt% total pigments in red meat.[46] Two to six wavelengths and their ratios extracted from satellite HSI images were applied in successive projections algorithms to quantify Chl-*a* concentration in natural waters within 3.05–0.174 wt%[47] and 1.96×10^{-5}–1.12×10^{-7} wt% ranges.[48] Similar relative absorption band ratios were used to quantify Chl-*a* and pheophytin-*a* of algae in lakes within the 0.11–2.80×10^{-4} wt% range.[49] Most of these algorithms output a finite number (bins) of predefined concentrations or ignore most of the available data. Although suitable for many applications, there is a need for concentration determination algorithms as continuous functions for detection of, e.g., pigments, hazardous compounds or other additives in plastics. To the best of our knowledge, no studies have developed models for in-line quantification of pigments in plastics using HSI techniques. Thus, new approaches are needed for determination of pigment concentrations via machine learning.

Blue colour or shades is one of the most common colours in ocean plastic waste (9 %) at global scale[50] and in this study a series of blue coloured (single pigment) samples will be compounded and investigated in a broad spectral range covering HSI in the visible (450–1050 nm) and SWIR (955–1700 nm) spectral ranges. The samples cover a broad pigment concentration interval ranging from 40 wt% to 1.7×10^{-3} wt% in LDPE and the chemical structures of pigment and plastics are verified by attenuated total reflectance (ATR)-FT-IR. The data will be modelled with both a peak ratio (of selected bands) model and a PC-based model using the full spectrum, subsequently predictive models are fitted for continuous concentration estimation. Finally, unknown concentrations of blue pigment in LDPE will be predicted based on the models.

Materials and methods

Sample preparation

Masterbatch (MB, 15-2040-PB-15-B, Kunstof-Kemi Skandinavia A/S, Denmark) with 40 wt% Organic C.I. Pigment Blue 15:3 (PB, Copper (II) phthalocyanine, $C_{32}H_{16}CuN_8$, CAS 147-14-8) in low density polyethylene (LDPE) was used for the preparation of a series of samples with a varying pigment concentration. LDPE (Eltex® MED PH23H630, INEOS Olefins and Polymer Europe) was used to dilute the masterbatch and obtain a blue colour gradient. Samples were prepared in a conical co-rotating twin-screw compounder with a backflow channel (Rheomex CTW5, MiniLab HAAKE), at 210 °C and 50 rpm for ≈7 min. The first two loads contained 10 wt% pigment (1st: 1 g MB and 3 g LDPE, 2nd: 0.75 g MB and 2.25 g LDPE). Then ten different concentrations were obtained by mixing pure LDPE (3 g LDPE loads) with the previous pigment concentration. The loaded and unloaded masses were determined (Sartorius QUINTIX224-1S, Sartorius Lab Instruments, Germany) and the mass balance, given in Supplementary Information (SI) Equation (S1)–(S6), were applied for calculation of the pigment concentrations. Samples with pigment concentrations of 40 (MB), 10, 4.5, 2.0, 0.83, 0.35, 0.15, 60×10^{-3}, 24×10^{-3}, 10×10^{-3}, 4.0×10^{-3}, 1.7×10^{-3} and 0 (LDPE) wt% was compounded. A schematic of the compounder, image of representative samples and molecular structure of the PB are shown in SI section S1. Test samples of 19.99, 15.18, 10.05, 5.19, 2.43, 1.04 and 0.31 wt% pigment concentration were manufactured by mixing LDPE and PB MB ($m_{LDPE}:m_{MB}$) 1.01 : 1.01, 1.24 : 0.76, 1.51 : 0.51, 1.75 : 0.26, 1.89 : 0.12, 1.95 : 0.05 and 1.99 : 0.03, respectively. The mixtures were compounded as already described, extruded and the compounder was cleaned between batches.

Attenuated total reflection Fourier-transform infrared spectroscopy

All samples were analysed with attenuated total reflectance Fourier-transform infrared spectroscopy (ATR-FT-IR) (Nicolet iS5 iD5 ATR, Thermo Scientific) with a ZnSe crystal (iTR/iD5, Thermo). Background measurement with 16 scans was obtained and refreshed every 20 min. FT-IR spectra were obtained with 32 scans for each sample with a resolution of 2 cm^{-1}. Spectra were corrected for penetration depth by advanced ATR followed by a baseline correction in OMNIC™ Spectra Software (Thermo Fisher).

Hyperspectral imaging

The hyperspectral imaging system (Newtec, Denmark) consists of hyperspectral cameras positioned 55 cm above a conveyor belt (29 cm wide, speed 3.75 m min^{-1}) transporting the samples. The illumination of the conveyor belt was done by two units of four halogen lamps (12 V, 20 W) placed 30 cm above the conveyor belt at a 45° angle. The line scan hyperspectral camera is equipped with two Oculus QT5022 detectors: Gsense scientific metal-oxide-semiconductor, CMOS, for the Vis/NIR region (from 450 nm to 1050 nm) and InGaAs for the SWIR region (from 955 nm to 1700 nm). The HSI system was controlled by the onboard software (Newtec, Denmark). Prior to measurement, a full spatial, spectral and intensity calibration was performed as previous described.[51] In short; a measurement on a calibration board containing a chess-pattern, LEDs and TiO_2 powder giving the calibration parameters. The spatial resolution is 0.22 nm (across) by 0.50 nm (along) for Vis/NIR and 1.10 mm (across) by 0.50 mm (along) for SWIR. The spectral resolution is 1.75 nm for Vis/NIR and 8.90 nm for SWIR. Intensity calibration was referenced to TiO_2. All spectral calibration details are given in SI section S3.

In a typical measurement, a row of samples was placed on the conveyor belt, passed the line scanner and the data cube was obtained. Each recording involved the sequential acquisition of 376,800 spectra (300 lines of 1256 pixels) for the Vis/NIR and 76,800 spectra (300 lines of 256 pixels) for the SWIR. Each pixel contains 350 and 110 spectral channels (λ) creating data cubes (x, y, λ) with dimensions (300, 1256, 350) and (300, 256, 110) for Vis/NIR and SWIR, respectively.

Hyperspectral data processing

The data cubes are transferred from the HSI cameras to an external computer for data processing. Spectra used for modelling are extracted from five regions of interest on each sample measuring 6 × 20 pixels and 6 × 7 pixels for Vis/NIR and SWIR, respectively. The reported spectrum for each sample is the total average of 600 or 210 spectra for Vis/NIR or SWIR, respectively.

The peak ratio model

For Vis/NIR, the LDPE band (CH_2, at 1030 nm, internal reference) is numerical integrated from 875 nm to 970 nm and the pigment peak is integrated from 550 nm to 800 nm. For SWIR, the combination bands (internal reference) are integrated from 1350 nm to 1620 nm and the pigment band is integrated from 1040 nm to 1145 nm. The calculated areas are baseline corrected over the given range via a linear function for both Vis/NIR and SWIR, and the peak ratio is calculated as pigment area divided by internal reference area. Pigment concentrations (Conc) are modelled as a function of peak ratios with an exponential function [Equation (1)] in a semi logarithmic plot [peak ratio vs Ln (Conc)].

$$\mathrm{Conc}(x) = Ae^{\tau x} \tag{1}$$

where A is the pre-exponential constant, τ is the exponent constant and x the model dependant variables.

All calculations were performed in Python (version 3.8).

The PCA model

In this approach PCA is first applied to reduce data dimensionality and eliminate the multicollinearity of the original qualitative HSI spectrum. This gives a new set of quantitative variables [principal component (PC) scores] which are orthogonal to each other. Subsequently, regression on the quantitative data (PC scores) is performed giving a continuous concentration model. The continuous extracted spectra are pre-processed with a Savitzky–Golay filter (SG, 7-point average, 2nd order polynomial, 1st order derivative) and followed by data normalisation (between 0 and 1) for the lowest and highest measured value. The data is then processed via PCA with four PCs. The second principal component (PC2) was applied for pigment concentration modelling in the Vis/NIR as reflections and scattering is dominating the first principal component (PC1). The first principal component (PC1) was used for pigment concentration modelling in the SWIR. Pigment concentrations are modelled as a function of PC with an exponential function [Equation (1)] in a semi logarithmic plot [PC *vs* Ln (Conc)]. All calculations were performed in Python (version 3.8).

Model testing

The peak ratio and PC-based models in Vis/NIR and SWIR are tested within their ranges by test samples having 20–0.31 wt% PB. The test samples are pre-processed accordingly, and the concentrations of PB are determined by the models. The linear fit between the expected and model predicted concentrations are calculated and reported as the coefficient of determination (R^2).

Results

Material validation

The compounded samples were extruded 5 mm wide and 2 mm thick and without sign of degradation or yellowing after compounding. An image of the samples can be found in Figure 1. Visual inspection of samples shows that the pigments are well and homogeneously distributed in the entire sample.

The ATR-FT-IR spectra for all samples are illustrated in Figure 2. The spectra in Figure 2 (individual spectra are shown in SI S2) are assigned to **LDPE**: CH_2 stretch (ν) bands at 2915 cm^{-1} and 2850 cm^{-1} and CH_2 bending (δ) bands at 1472, 1465, 730 and 720 cm^{-1}.[52] **Pigment**: The Copper (II) phthalocyanine pigment (SI S3) adds absorption bands to the MB spectrum and coloured samples. Bands at 1608, 1505, 1287, 1174, 1165, 900 and 878 cm^{-1} are assigned to ν and δ of C–H and C=C from 1,2 disubstituted benzene. Bands from the tertiary amine in the porphyrin ring (νC–N) are observed at 1120–1065 cm^{-1}.[52,53] Bands at 1608, 1505, 1420 and 1320 cm^{-1} are assigned to C=C and C–N vibrations of the porphyrin ring.[54,55] The band from bending out of plane for 1,2 substituted aromat from phthalocyanine. This band overlays with the band from LDPE (CH_2, doublet

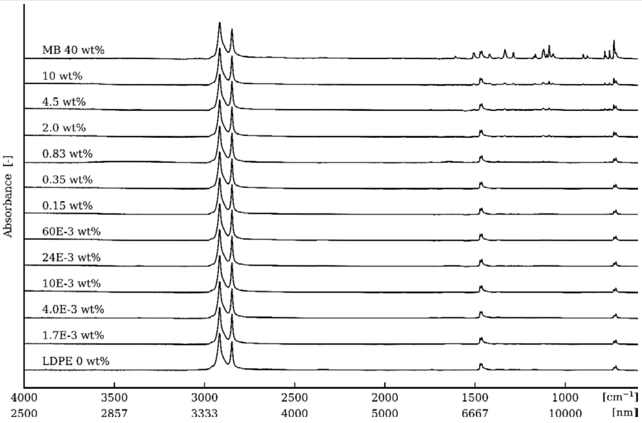

Figure 2. ATR-FT-IR spectra for the applied materials. The spectra are stacked by shifting the absorbance for visual clarity. Bands at 2340 cm^{-1} and 2365 cm^{-1} are assigned to atmospheric $^{\nu}CO_2$.

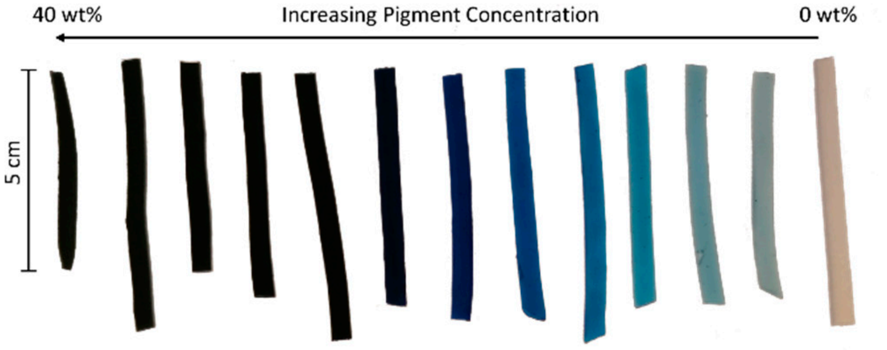

Figure 1. Image of the specimens with concentrations of pigment from left (40 wt%) to right (1.7×10^{-3} wt%) and on the right virgin LDPE.

band) at 730 cm^{-1} giving a significant intensity increases. Finally, the Cu(II) phthalocyanine is indicated by the weak band at 640 cm^{-1}.[54,55] The assignment verified the material and incorporated pigment but is not a quantitative measurement of the concentration.

Hyperspectral characterisation via Vis/NIR and SWIR

The Vis/NIR spectrum for the samples are given in Figure 3. The hyperspectral image representation of the samples and the individual and detailed Vis/NIR spectra are given in SI S4.

In the Vis/NIR spectral region (Figure 3), the concentrated blue samples absorb most of the irradiated light making them appear dark and thus no clear spectral features can be observed. However, as the pigment concentration decreases absorption bands appear at 550–760 nm indicating absorption of all colours expect blue.[56] In the lower concentration range (4.0 × 10^{-3} and 1.7 × 10^{-3} wt%) an absorbance band at 680 nm arises which is assigned to the blue colour.[56]

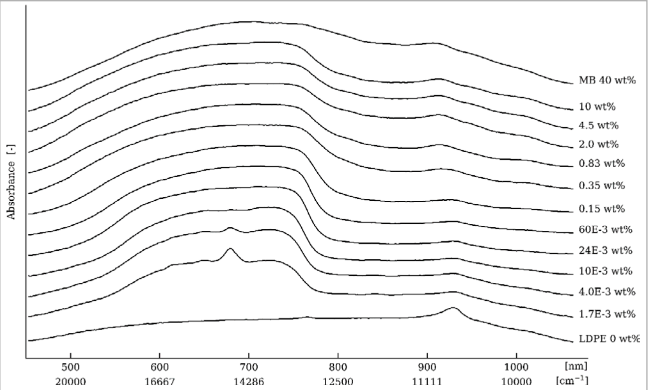

Figure 3. Vis/NIR hyperspectral spectra for the applied samples. The spectra are (for clarity) plotted with upshifted absorbance having the masterbatch most shifted and LDPE non-shifted. Each spectrum is an average of 600 pixels.

The spectral information for the SWIR wavelengths is shown in Figure 4. The hyperspectral image representation of the samples and the individual SWIR samples can be found in SI S4. The bands from the LDPE at 1226 nm are ascribed to 3vCH$_2$/CH, bands at 1042, 1430 and 1459 nm are ascribed to the combination bands from 3vCH$_2$ and δCH$_2$. The bands at 1703 nm and 1729 nm are ascribed to 2vCH$_3$/CH$_2$ overtones. The bands at 1042 nm and 1703 nm are ascribed to C-H in LDPE.[57] The MB spectrum is a combination of LDPE and the pigment, thus having the LDPE bands as described above and additional bands at 1016 nm and 1088 nm which are assigned to aromatic 3vCH. Further, a weak signal at 1690 nm appears in the samples with 40 wt% and 10 wt% from aromatic C–H.[57]

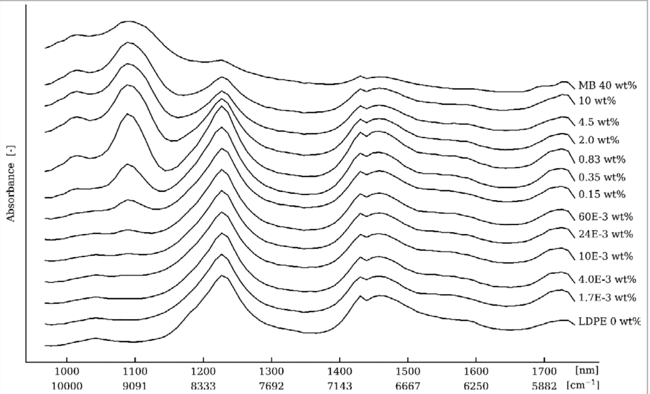

Figure 4. SWIR hyperspectral spectra for the applied samples. The spectra are (for clarity) plotted with upshifted absorbance having the masterbatch most shifted and LDPE non-shifted. Each spectrum is an average of 210 pixels.

Concentration estimation

The first approach is to apply the models to the whole dynamic range from 40.0 wt% to 0.0 wt% (SI S5) and based on outcome interpretation it was found that Vis/NIR performs best at diluted concentrations of PB due to sensor saturation at higher concentrations. On the other hand, SWIR performs better at higher concentrations as the chemical signatures of PB are more pronounced. After optimisation iterations the final peak ratio and PC-based models (see SI S5 for details) for concentration estimation are shown in Figure 5.

The peak ratio model in Vis/NIR has a predictive range from 60 × 10^{-3} wt% to 1.7 × 10^{-3} wt% PB (Figure 5 top, left), whereas the PC-based model is performed in the range from 0.83 wt% to 1.7 × 10^{-3} wt% PB (Figure 5 bottom, left). SWIR is more capable at higher concentrations, and the ratio model performs well in the range from 40.0 wt% to 0.15 wt% PB (Figure 5 top, right), while the PC-based model performs in the range from 40.0 wt% to 60 × 10^{-3} wt% PB (Figure 5 bottom, right). The test samples predicting wt% can be found in Table 1. From Figure 5 and Table 1 it is observed that the peak ratio has more scatter and a lower interval for usage than for the PC-based method, although both modelling approaches can model the entire pigment range when Vis/NIR and SWIR is combined.

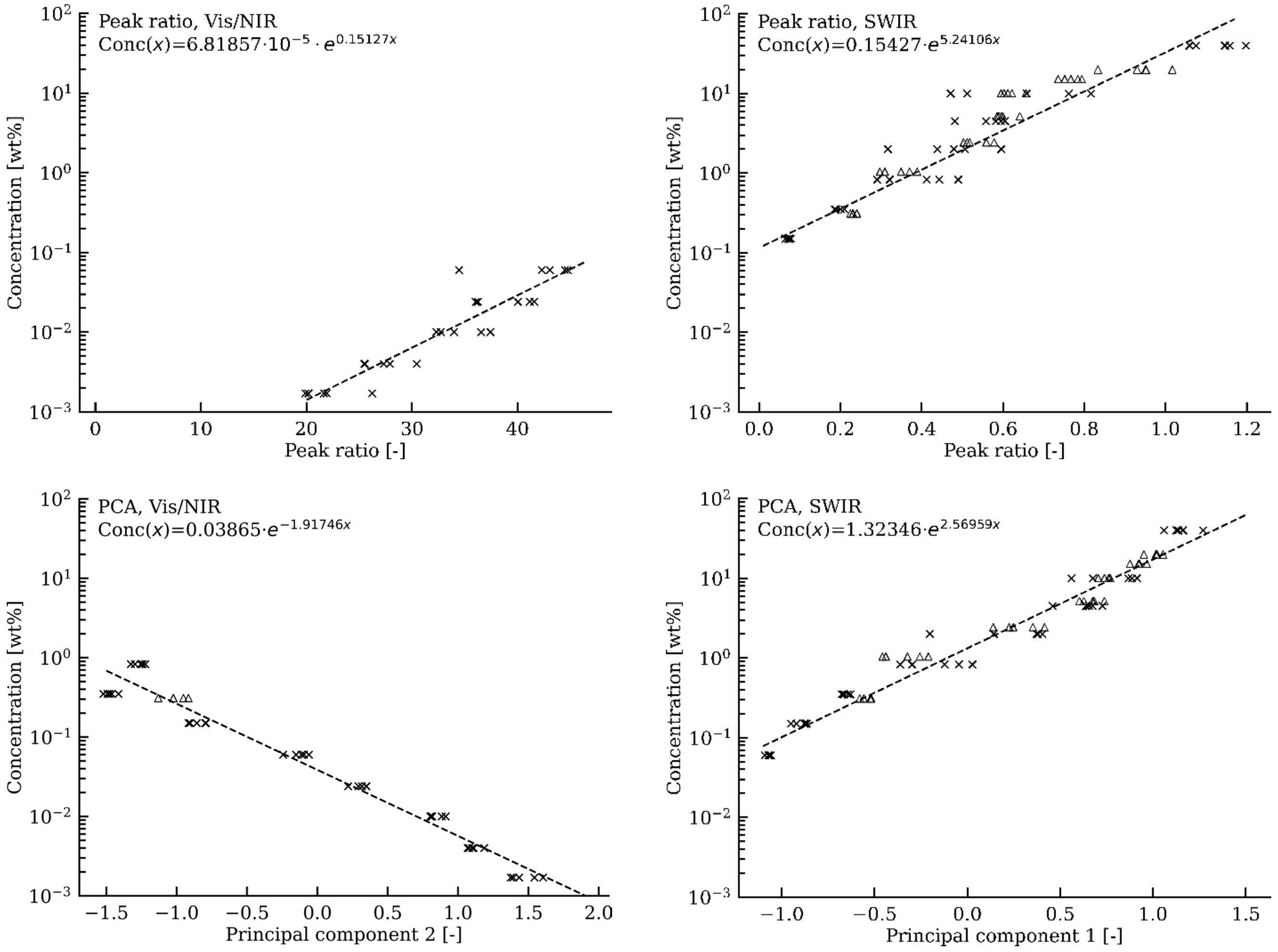

Figure 5. Pigment concentration estimation from peak ratio (top row) and PC-based modelling (bottom row) for Vis/NIR (left column) and SWIR (right column). Model data (×), test data (Δ) and the dashed line is the model.

Discussion

The dilution series of PB in LDPE is made from a master batch containing 40 wt% pigment and is diluted to 1.7×10^{-3} wt% pigment. Homogeneous mixing is assumed when diluting, and the concentrations of the samples are calculated based on the mass balance, where a part of the total mass stay in the compounder and is diluted by an addition of pure LDPE. The mass balance is considered more accurate compared to adding LDPE and MB to the compounder in a batch, even when minor differences in the master batch loading or variances in the carry over mass is considered. The batch mode struggle, if ± one MB pellet (~25 mg) is loaded to the compounder for a desired concentration of 1.04 wt% (1.985 g LDPE, 0.052 g MB), giving deviations of almost ±25 %. Further, only a fraction of a MB pellet is to be added if even lower concentrations are to be obtained. In addition, an unknown amount of material ends in dead zones during mixing, which is crucial for a batch, but is considered constant in a dilution series. The dead zone effect is minimised by loading half of the LDPE to the compounder, then the pigment and then the second half of LDPE. In any case training data is made via the dilution series and test samples are made via batch mode to test the model on samples made differently. However, lower pigment concentrations could not be reliable produced in batch mode which limits the test samples to 19.99, 15.18, 10.05, 5.19, 2.43, 1.04 and 0.31 wt% PB.

The FT-IR spectra clearly verified the polymer to be LDPE and the presence of Copper (II) phthalocyanine in different loadings based on corresponding peak intensities. Especially the νC–N observed at 1120–1065 cm^{-1} are significant when differentiating between LDPE and PB. Copper (II) phthalocyanine was found to absorb light in the range from 550 nm to 760 nm in the Vis/NIR and the spectral range narrows as pigment loading decreases and a band apex is found at 680 nm at PB loadings for

Table 1. Test samples predicted concentrations according to the models. The peak ratio model uses the concentrations intervals from [0.06;0.0017] wt% and [40.0;0.15] wt% for Vis/NIR and SWIR, respectively. The PC-based model uses the concentrations intervals from [0.83;0.0017] wt% and [40.0;0.06] wt% for Vis/NIR and SWIR, respectively.

Conc (wt%)	Vis/NIR[a] (wt%)	SWIR[a] (wt%)[c]	Vis/NIR[b] (wt%)	SWIR[b] (wt%)[d]
19.99	–	23.83 ± 8.11	–	17.86 ± 1.67
15.18	–	8.82 ± 1.15	–	14.19 ± 1.17
10.05	–	3.84 ± 0.54	–	8.91 ± 0.57
5.19	–	3.53 ± 0.47	–	7.32 ± 1.01
2.43	–	3.42 ± 0.46	–	2.69 ± 0.78
1.04	–	0.84 ± 0.18	–	0.56 ± 0.16
0.31	–	0.45 ± 0.02	0.27 ± 0.04	0.32 ± 0.02

[a]Peak ratio model, [b]PC-based model, [c]R^2 = 0.7896, [d]R^2 = 0.9773

4.0×10^{-3} wt% and 1.7×10^{-3} wt%. For SWIR, LDPE is clearly identified at 1042, 1226, 1430 and 1459 nm and PB at 1016 nm and 1088 nm. Where the signal at 1088 nm correlates with the expected pigment loadings. Concentrations from 60×10^{-3} wt% and above is sufficient to differentiate PB based on the spectra alone and spectra at concentrations of 24×10^{-3} wt% and below appear as LDPE. Hence, all spectral ranges (Vis/NIR, SWIR and ATR-FT-IR) confirm that Copper (II) phthalocyanine is present in LDPE at varying concentrations.

The concentration determination in HSI from integration is in general challenged by uneven illumination, sample curvature, reflections and the light intensity reaching the cameras cannot be assumed to be constant. Hence, the measurements in its raw format are considered as qualitative results. This is addressed by using the bands (1030 nm Vis/NIR and 1450 nm in the SWIR) from LDPE as pseudo internal reference in the peak ratio model, enabling extraction of relative quantitative information from the obtained spectra. This approach has an inherited error as the high PB loadings will also dilute the LDPE loading and the higher concentrations (5 wt%+) are artificially amplified. At high PB loading the bands are broadened enforcing wide boundaries to be set. However, at the lower concentrations the broad boundaries challenge the integration by lowering the signal-to-noise ratio, giving poorly defined baselines, increasing data variance and lowered detection limits to 60×10^{-3} wt%. Although a direct method it has some challenging drawbacks. The peak ratio model managed to cover from 60×10^{-3} wt% to 1.7×10^{-3} wt% in Vis/NIR and 40.0–0.15 wt% in SWIR and generates fair to poor concentration predictions ($R^2 = 0.7896$ between calculated and predicted pigment wt%).

As an alternative, the PC-based model will model the different concentrations via their variances over the entire dataset, while also adjusting for a potential spectral overlapping. PCA is more noisy and intensity sensitive which can be surcompassed by using the SG filter with a soft smoothing and calculating the first derivative to address the challenges of noise and intensity, respectively. The PC-based model reached an upper detection limit of 0.15 wt% in the Vis/NIR region despite the low penetration depth[58] and reduced light reflection[59] of high concentration samples. In contrast, the SWIR region verified the deeper penetration[60] and distinguished pigment concentrations up to 40 wt% and a lower detection limit of 60×10^{-3} wt%. The PC-based model thus renders a fair to good concentration prediction ($R^2 = 0.9773$ between calculated and predicted pigment wt%).

It is clear from Figure 5 that neither vis/NIR nor SWIR can be applied alone for concentration estimation over the four orders of magnitude. The Vis/NIR experience, a saturation level beyond which no correlation with increasing concentration is seen (SI S5). Whereas, SWIR has a lower detection limit where the signal from LDPE overwhelms the spectral information of PB (SI S6). The PC-based models expanded the applicable range for both HSI systems and showed that Vis/NIR and SWIR data of PB in plastic samples are complementary, with a good separation of low concentrations in the Vis/NIR and high concentrations in the SWIR, and that it combined provides a full and reliable detection of the PB concentration range from 40 wt% to 1.7×10^{-3} wt% in LDPE. In addition, most industrial applications have pigment loadings below 4 wt% and thus the models fall in the valid concentration range. Even though the proposed models predict the pigment concentration of PB in LDPE, it is important to note that calibration of both model and equipment are necessary. In some applications the equipment calibration could be minimised to intensity calibration and then fit the models to the HSI system readout. In addition to equipment calibration, it is important to have calibration materials with known pigment concentrations over the range of interest and in the material (e.g., polypropylene, polystyrene, polyamide etc.) of interest. Hence, the obtained models are system specific and can only be interpolated within the calibrated pigment range. However, in-line estimations of pigment concentration are enabled after accurate equipment and model calibration. There are several industrial applications that can benefit from continuous in-line prediction of pigment concentrations. A few examples could be estimated for amount of necessary pigment to add for obtaining the right product colour within the textile recycling industry. In the plastic recycling industry, the clear benefit is product documentation and for pigment dosing applications. In general application to product surveillance in production facilities for quality control assurance.

Conclusion

In this study, a hyperspectral imaging system covering both the Vis/NIR and SWIR spectral ranges was employed for predicting pigment blue 15:3 concentrations in LDPE. The spectra showed an upper detection limited of 0.83 wt% pigments for Vis/NIR and lower detection limited of 60 wt% pigments for SWIR. The machine learning utilises all variances found in the continuous spectra via a PCA model and subsequently fits a mathematical function to the output to predict the pigment concentration via continuous functions. The combined spectral ranges give full information of concentration ranging from 40.0 wt% to 1.7×10^{-3} wt% pigment loadings with a $R^2 = 0.9773$ between calculated and predicted pigment loadings—hence industrial in-line concentration determination over four orders of magnitude. The proposed method is a fast, non-destructive and inexpensive way for measuring the pigment content of plastics during recycling, providing an alternative to the traditional methods.

Acknowledgements

The authors thank Celine B. Karlsen, Aarhus University for help with data processing. The authors also thank the Innovation Fond Denmark (grant no: 0177-00035A), Aarhus University, Dansk Affaldsminimering, Vestforbrænding, and Plastix for financial support under the Re-Plast project.

Credit

Georgiana Amarie: Investigation, Formal analysis, Writing - Original Draft, Writing - Review & Editing, Visualisation. **Anne Sofie Schaarup-Kjær**: Conceptualisation, Methodology, Investigation, Formal analysis, Writing - Review & Editing, Visualisation. **Pernille Klarskov**: Funding acquisition. **Martin Lahn Henriksen**: Conceptualisation, Software, Funding acquisition, Supervision, Writing - Review & Editing. **Mogens Hinge**: Conceptualisation, Supervision, Funding acquisition, Project administration, Software, Writing - Original Draft, Writing - Review & Editing, Visualisation.

References

1. I. Auken, "Danmark uden affald", *Miljø- og Fødevareministeriet* **14(2),** 1 (2013).
2. F. Besenbacher, "Advisory board for cirkulær økonomi - anbefalinger til regeringen", *Miljø- og Fødevareministeriet* 1 (2017).
3. G. Leone, J.M.T. Borràs, E. de V. Martín and Ellen MacArthur Foundation, "The new plastics economy: rethinking the future of plastics & catalysing action", *Ellen MacArthur Found.* **68** (2017).
4. S.A. Veltzé, C. Fischer and S. Hirsbak, "Miljøets fodspor nr. 5 – affald", *Miljøstyrelsen* **(5),** 1 (2019).
5. D.K.A. Barnes, A. Walters and L. Gonçalves, "Macroplastics at sea around antarctica", *Mar. Environ. Res.* **70(2),** 250 (2010). https://doi.org/10.1016/j.marenvres.2010.05.006
6. A.S. Colferai, R.P. Silva-Filho, A.M. Martins and L. Bugoni, "Distribution pattern of anthropogenic marine debris along the gastrointestinal tract of green turtles (*Chelonia mydas*) as implications for rehabilitation", *Mar. Pollut. Bull.* **119(1),** 231 (2017). https://doi.org/10.1016/j.marpolbul.2017.03.053
7. P.L. Corcoran, M.C. Biesinger and M. Grifi, "Plastics and beaches: a degrading relationship", *Mar. Pollut.*

Bull. **58(1),** 80 (2009). https://doi.org/10.1016/j.marpolbul.2008.08.022

8. E. Martinez, K. Maamaatuaiahutapu and V. Taillandier, "Floating marine debris surface drift: convergence and accumulation toward the South Pacific subtropical gyre", *Mar. Pollut. Bull.* **58(9),** 1347 (2009). https://doi.org/10.1016/j.marpolbul.2009.04.022
9. P.G. Ryan, C.J. Moore, J.A. Van Franeker and C.L. Moloney, "Monitoring the abundance of plastic debris in the marine environment", *Philos. Trans. R. Soc. B Biol. Sci.* **364(1526),** 1999 (2009). https://doi.org/10.1098/rstb.2008.0207
10. SUSCHEM, *Sustainable Plastics Strategy* (2020).
11. R.C. Thompson, Y. Olson, R.P. Mitchell, A. Davis, S.J. Rowland, A.W.G. John, D. McGonigle and A.E. Russell, "Lost at sea: where is all the plastic?", *Science* **304(5672),** 838 (2004). https://doi.org/10.1126/science.1094559
12. European Comission, "A european strategy for plastics in a circular economy", *Eur. Comm.* (2018).
13. P.H. Andersen, T. Duvold, B. Frølund, J. Lüneborg, K. Toft-Petersen, H. Vanthournout and C. Witte, *The New Plastics Economy* **January** (2019).
14. M. Tsakona and I. Rucevska, "Baseline report on plastic waste", *Basel Conv.* 1 (2020).
15. Indriatmoko, Y. Shioi, T.H.P. Brotosudarmo and L. Limantara, "Separation of photosynthetic pigments by high-performance liquid chromatography: comparison of column performance, mobile phase, and temperature", *Procedia Chem.* **14,** 202 (2015). https://doi.org/10.1016/j.proche.2015.03.029
16. I. Degano, F. Modugno, I. Bonaduce, E. Ribechini and M.P. Colombini, "Recent advances in analytical pyrolysis to investigate organic materials in heritage science", *Angew. Chemie - Int. Ed.* **57(25),** 7313 (2018). https://doi.org/10.1002/anie.201713404
17. M.R. Derrick, D. Stulik and J.M. Landry, *Infrared Spectroscopy in Conservation Science*, **3(April).** The Getty Conservation Institute, United States of America (1955).
18. A. Vila, N. Ferrer and J.F. García, "Chemical composition of contemporary black printing inks based on infrared spectroscopy: basic information for the characterization and discrimination of artistic prints", *Anal. Chim. Acta* **591(1),** 97–105 (2007). https://doi.org/10.1016/J.ACA.2007.03.060
19. C. Genestar and C. Pons, "Earth pigments in painting: characterisation and differentiation by means of FTIR spectroscopy and SEM-EDS microanalysis", *Anal. Bioanal. Chem.* **382(2),** 269–274 (2005). https://doi.org/10.1007/S00216-005-3085-8
20. X. Li, J. Jin, C. Sun, D. Ye and Y. Liu, "Simultaneous determination of six main types of lipid-soluble pigments in green tea by visible and near-infrared spectroscopy", *Food Chem.* **270,** 236–242 (2019). https://doi.org/10.1016/J.FOODCHEM.2018.07.039
21. L. Zhang, H. Ding, Y. Wang, X. Guo and H. Li, "Performance of calibration model with different ratio of sample size to the number of wavelength: application to hemoglobin determination by NIR spectroscopy", *Spectrochim. Acta A* **227,** 117750 (2020). https://doi.org/10.1016/J.SAA.2019.117750
22. H.G.M. Edwards and J.M. Chalmers (Eds), *Raman Spectroscopy in Archaeology and Art History.* Royal Society of Chemistry (2005).
23. J. van der Weerd, G.D. Smith, S. Firth and R.J.H. Clark, "Identification of black pigments on prehistoric southwest American potsherds by infrared and Raman microscopy", *J. Archaeol. Sci.* **31(10),** 1429–1437 (2004). https://doi.org/10.1016/j.jas.2004.03.008
24. Z. feng Liu, H. Zhang, W. hua Zhou, S. Cai Hao, Z. Zhou, X. Kun Qi and J. Long Shi, "Pigment identification on an undated Chinese painting by non-destructive analysis", *Vib. Spectrosc.* **101,** 28–33 (2019). https://doi.org/10.1016/j.vibspec.2018.08.009
25. A. Romani, C. Clementi, C. Miliani and G. Favaro, "Fluorescence spectroscopy: a powerful technique for the noninvasive characterization of artwork", *Acc. Chem. Res.* **43(6),** 837–846 (2010). https://doi.org/10.1021/ar900291y
26. L. Ravikanth, D.S. Jayas, N.D.G. White, P.G. Fields and D.-W. Sun, "Extraction of spectral information from hyperspectral data and application of hyperspectral imaging for food and agricultural products", *Food Bioprocess Technol.* **10(1),** 1–33 (2017). https://doi.org/10.1007/s11947-016-1817-8
27. X. Yu, H. Lu and Q. Liu, "Deep-learning-based regression model and hyperspectral imaging for rapid detection of nitrogen concentration in oilseed rape (*Brassica napus* L.) leaf", *Chemometr. Intell. Lab. Syst.* **172,** 188–193 (2018). https://doi.org/10.1016/j.chemolab.2017.12.010
28. G. Kim, H. Lee, I. Baek, B.K. Cho and M.S. Kim, "Quantitative detection of benzoyl peroxide in wheat flour using line-scan short-wave infrared hyperspectral imaging", *Sensors Actuators B Chem.*

352(P1), 130997 (2022). https://doi.org/10.1016/j.snb.2021.130997

29. G. Lu and B. Fei, "Medical hyperspectral imaging: a review", *J. Biomed. Opt.* **19(1),** 010901 (2014). https://doi.org/10.1117/1.JBO.19.1.010901
30. Y. Zheng, J. Bai, J. Xu, X. Li and Y. Zhang, "A discrimination model in waste plastics sorting using NIR hyperspectral imaging system", *Waste Manag.* **72,** 87–98 (2018). https://doi.org/10.1016/j.wasman.2017.10.015
31. S. Serranti, A. Gargiulo and G. Bonifazi, "Characterization of post-consumer polyolefin wastes by hyperspectral imaging for quality control in recycling processes", *Waste Manag.* **31(11),** 2217–2227 (2011). https://doi.org/10.1016/j.wasman.2011.06.007
32. M.L. Henriksen, C.B. Karlsen, P. Klarskov and M. Hinge, "Plastic classification via in-line hyperspectral camera analysis and unsupervised machine learning", *Vib. Spectrosc.* **118,** 103329 (2022). https://doi.org/10.1016/j.vibspec.2021.103329
33. G. Bonifazi, G. Capobianco and S. Serranti, "A hierarchical classification approach for recognition of low-density (LDPE) and high-density polyethylene (HDPE) in mixed plastic waste based on short-wave infrared (SWIR) hyperspectral imaging", *Spectrochim. Acta A* **198,** 115–122 (2018). https://doi.org/10.1016/j.saa.2018.03.006
34. O. Rozenstein, E. Puckrin and J. Adamowski, "Development of a new approach based on midwave infrared spectroscopy for post-consumer black plastic waste sorting in the recycling industry", *Waste Manag.* **68,** 38–44 (2017). https://doi.org/10.1016/j.wasman.2017.07.023
35. B. Grabowski, W. Masarczyk, P. Głomb and A. Mendys, "Automatic pigment identification from hyperspectral data", *J. Cult. Herit.* **31,** 1–12 (2018). https://doi.org/10.1016/j.culher.2018.01.003
36. T. Cavaleri, A. Giovagnoli and M. Nervo, "Pigments and mixtures identification by visible reflectance spectroscopy", *Procedia Chem.* **8,** 45–54 (2013). https://doi.org/10.1016/j.proche.2013.03.007
37. A. Cosentino, "Identification of pigments by multispectral imaging; a flowchart method", *Herit. Sci.* **2,** 8 (2014). https://doi.org/10.1186/2050-7445-2-8
38. C. Balas, G. Epitropou, A. Tsapras and N. Hadjinicolaou, "Hyperspectral imaging and spectral classification for pigment identification and mapping in paintings by El Greco and his workshop", *Multimed. Tools Appl.* **77,** 9737–9751 (2018). https://doi.org/10.1007/s11042-017-5564-2
39. F. Grillini, J. Thomas and S. George, "VisNIR pigment mapping and re-rendering of an experimental painting", *J. Int. Colour Assoc.* **26,** 3–10 (2021).
40. W. Jang, Y. Park, J. Pyo, S. Park, J. Kim, J.H. Kim, K.H. Cho, J.K. Shin and S. Kim, "Optimal band selection for airborne hyperspectral imagery to retrieve a wide range of cyanobacterial pigment concentration using a data-driven approach", *Remote Sens.* **14(7),** 1 (2022). https://doi.org/10.3390/rs14071754
41. X. Li, K. Chen and Y. He, "*In situ* and non-destructive detection of the lipid concentration of *Scenedesmus obliquus* using hyperspectral imaging technique", *Algal Res.* **45(July 2019),** 101680 (2020). https://doi.org/10.1016/j.algal.2019.101680
42. Y.R. Zhao, X. Li, K.Q. Yu, F. Cheng and Y. He, "Hyperspectral imaging for determining pigment contents in cucumber leaves in response to angular leaf spot disease", *Sci. Rep.* **6,** 27790 (2016). https://doi.org/10.1038/srep27790
43. S. Chen, F. Zhang, J. Ning, X. Liu, Z. Zhang and S. Yang, "Predicting the anthocyanin content of wine grapes by NIR hyperspectral imaging", *Food Chem.* **172,** 788 (2015). https://doi.org/10.1016/j.foodchem.2014.09.119
44. Y.C. Yang, D.W. Sun, H. Pu, N.N. Wang and Z. Zhu, "Rapid detection of anthocyanin content in lychee pericarp during storage using hyperspectral imaging coupled with model fusion", *Postharvest Biol. Technol.* **103,** 55 (2015). https://doi.org/10.1016/j.postharvbio.2015.02.008
45. M.P. Diago, J. Fernández-Novales, A.M. Fernandes, P. Melo-Pinto and J. Tardaguila, "Use of visible and short-wave near-infrared hyperspectral imaging to fingerprint anthocyanins in intact grape berries", *J. Agric. Food Chem.* **64(40),** 7658 (2016). https://doi.org/10.1021/acs.jafc.6b01999
46. Z. Xiong, D.W. Sun, A. Xie, H. Pu, Z. Han and M. Luo, "Quantitative determination of total pigments in red meats using hyperspectral imaging and multivariate analysis", *Food Chem.* **178,** 339 (2015). https://doi.org/10.1016/j.foodchem.2015.01.071
47. H. Tian, C. Cao, M. Xu, Z. Zhu, D. Liu, X. Wang and S. Cui, "Estimation of chlorophyll-*a* concentration in coastal waters with HJ-1A HSI data using a three-band bio-optical model and validation", *Int. J. Remote Sens.* **35(16),** 5984 (2014). https://doi.org/10.1080/01431161.2014.934403

48. Z. Weng, J. Wang, T. Senthil and L. Wu, "Mechanical and thermal properties of abs/montmorillonite nanocomposites for fused deposition modeling 3D printing", *Mater. Des.* **102,** 276 (2016). https://doi.org/10.1016/j.matdes.2016.04.045
49. T. Schneider, D. Rimer, C. Butz and M. Grosjean, "A high-resolution pigment and productivity record from the varved Ponte Tresa basin (Lake Lugano, Switzerland) since 1919: insight from an approach that combines hyperspectral imaging and high-performance liquid chromatography", *J. Paleolimnol.* **60(3),** 381 (2018). https://doi.org/10.1007/s10933-018-0028-x
50. E. Martí, C. Martin, M. Galli, F. Echevarría, C.M. Duarte and A. Cózar, "The colors of the ocean plastics", *Environ. Sci. Technol.* **54(11),** 6594 (2020). https://doi.org/10.1021/acs.est.9b06400
51. M.L. Henriksen, W.N. Pedersen, P. Klarskov and M. Hinge, "One step calibration of industrial hyperspectral cameras", *Chemometr. Intell. Lab. Syst.* **227,** 104609 (2022). https://doi.org/10.1016/J.CHEMOLAB.2022.104609
52. G. Socrates, *Infrared and Raman Characteristic Group Frequencies*, 3rd Edn. John Wiley & Sons (2001).
53. J.E. McMurry, *Organic Chemistry*, 9th Edn. Cornell University (2015). ISBN: 9781305080485
54. G. Socrates, *Infrared and Raman Characteristic Group Frequencies: Tables and Charts*, 3rd Edn. John Wiley & Sons (2004).
55. A.A.M. Farag, "Optical absorption studies of copper phthalocyanine thin films", *Opt. Laser Technol.* **39(4),** 728 (2007). https://doi.org/10.1016/J.OPTLASTEC.2006.03.011
56. A.E. Owen, *Fundamentals of UV-Visible Spectroscopy.* Hewlett Packard (1996).
57. J. Workman Jr and L. Weyer, *Practical Guide and Spectral Atlas for Interpretive Near-Infrared Spectroscopy*, 2nd Edn. CRC Press (2012). https://doi.org/10.1201/b11894
58. N. Teraphongphom, C.S. Kong, J.M. Warram and E.L. Rosenthal, "Specimen mapping in head and neck cancer using fluorescence imaging", *Laryngoscope Investig. Otolaryngol.* **2(6),** 447 (2017). https://doi.org/10.1002/LIO2.84
59. H. Masoumi, S.M. Safavi and Z. Khani, "Identification and classification of plastic resins using near infrared reflectance spectroscopy", *Int. J. Mech. Mechatronics Eng.* **6(5),** 877 (2012). https://doi.org/10.5281/ZENODO.1076916
60. M. Manley, "Near-infrared spectroscopy and hyperspectral imaging: non-destructive analysis of biological materials", *Chem. Soc. Rev.* **43(24),** 8200 (2014). https://doi.org/10.1039/C4CS00062E